

# Horizontal shear wave scattering from a nonwelded interface observed by magnetic resonance elastography

S Papazoglou<sup>1</sup>, U Hamhaber<sup>2</sup>, J Braun<sup>2</sup> and I Sack<sup>1</sup>

<sup>1</sup> Department of Radiology, Charite University Hospital, Berlin, Germany

<sup>2</sup> Institute of Medical Informatics, Charite University Hospital, Berlin, Germany

E-mail: [ingolf.sack@charite.de](mailto:ingolf.sack@charite.de)

Received 15 June 2006, in final form 28 November 2006

Published 11 January 2007

Online at [stacks.iop.org/PMB/52/675](http://stacks.iop.org/PMB/52/675)

## Abstract

A method based on magnetic resonance elastography is presented that allows measuring the weldedness of interfaces between soft tissue layers. The technique exploits the dependence of shear wave scattering at elastic interfaces on the frequency of vibration. Experiments were performed on gel phantoms including differently welded interfaces. Plane wave excitation parallel to the planar interface with corresponding motion sensitization enabled the observation of only shear-horizontal (SH) wave scattering. Spatio-temporal filtering was applied to calculate scattering coefficients from the amplitudes of the incident, transmitted and reflected SH-waves in the vicinity of the interface. The results illustrate that acoustic wave scattering in soft tissues is largely dependent on the connectivity of interfaces, which is potentially interesting for imaging tissue mechanics in medicine and biology.

## 1. Introduction

The scattering of plane elastic waves by interfaces is of fundamental interest in seismology (Aki and Richards 2002) and medical imaging (Tribikram 2004). For example, the exploration of fractures and cracks in the Earth's upper crust is based on the scattering effects of seismic waves. In ultrasonic imaging, the scattering of elastic waves is directly related to the image contrast. In shear wave-based elastography as well (Lerner *et al* 1990, Muthupillai *et al* 1995, Sandrin *et al* 1999, Park and Maniatty 2006), the observation of scattering effects was reported in the context of MR elastography of the brain (Sack *et al* 2005, 2006). The analysis of elastic wave scattering in complex media suffers from multiple unknowns influencing the degree of wave reflection and transmission from elastic discontinuities. Particularly, in the presence of imperfectly bounded tissue layers, the degree of scattering is a function of

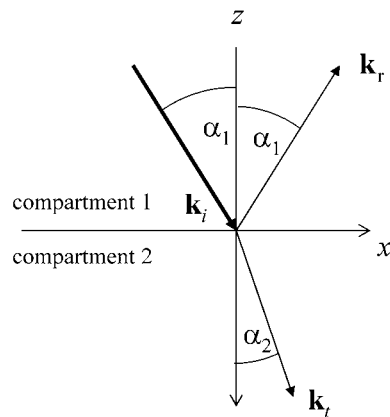


**Figure 1.** Sketch of an incident plane SH-wave (displacement is out of plane) with wave vector  $\mathbf{k}_i$  hitting a contact surface (at  $z = 0$ ) at an angle  $\alpha_1$ . Correspondingly, the wave vectors of the reflected and transmitted waves are labelled  $\mathbf{k}_r$  and  $\mathbf{k}_t$ .

the oscillation frequency of the elastic waves. This phenomenon was theoretically analysed by Schoenberg (1980), who provided explicit expressions for the reflection and transmission coefficients of shear-horizontal (SH) waves. Since then, several other groups have accounted for slip interfaces in theoretical or numerical studies in seismology and geophysics (e.g. Pyrak-Nolte *et al* (1990), Verweij and Chapman (1997), Chaisri and Krebes (2000), Slawinski and Krebes (2002)). These studies underscore the importance of considering the weldedness of connected media for correctly analysing acoustic wave scattering in composite materials. In this paper, we hypothesize that slip interfaces also play an important role in medical applications of acoustic waves. We therefore designed an interface-phantom that reproduces the elastic parameter range found by MR elastography (MRE) of living soft tissue. The acoustic response to the interface was quantified using shear vibrations at multiple driving frequencies between 50 and 400 Hz, as applicable for *in vivo* MRE studies. The unique ability of MRE to selectively encode specific wave field components enabled us to exclusively focus on SH-waves corresponding to out of plane motion sensitization. As we will demonstrate in this study, the degree of weldedness of soft elastic layers, quantitatively described by the specific stiffness  $\kappa$ , is well deducible from frequency-dependent SH-wave scattering observed in MR elastography.

## 2. Theory

Two homogeneous infinite isotropic half-spaces separated by a nonwelded planar interface are considered in the following. Cartesian coordinates are chosen such that the interface coincides with the  $xy$ -plane at  $z = 0$ . A plane wave travels in the positive  $z$ -direction hitting the interface at an angle  $\alpha_1$  inclined by its wave vector  $\mathbf{k}$  and the  $z$ -axis (figure 1). The wave vector is assumed to have no component pointing out of the  $xz$ -plane, while the polarization vector is parallel to the interface, thereby characterizing the elastic wave as an SH-wave. In scattering, it is useful to consider the inverse velocity or *slowness* instead of the wave vector, since the horizontal component  $p$  of the slowness is preserved during the scattering process. Since SH-waves only produce SH-waves upon scattering, the incident, reflected and transmitted

waves ( $\mathbf{u}_i$ ,  $\mathbf{u}_r$  and  $\mathbf{u}_t$ , respectively) can be expressed as

$$\begin{aligned}\mathbf{u}_i &= \exp \left[ i\omega \left( p \cdot x + \frac{\cos \alpha_1}{c_1} z - t \right) \right] \hat{\mathbf{y}}, \\ \mathbf{u}_r &= R \exp \left[ i\omega \left( p \cdot x - \frac{\cos \alpha_1}{c_1} z - t \right) \right] \hat{\mathbf{y}}, \\ \mathbf{u}_t &= T \exp \left[ i\omega \left( p \cdot x + \frac{\cos \alpha_2}{c_2} z - t \right) \right] \hat{\mathbf{y}},\end{aligned}\quad (1)$$

where  $\omega$  is the angular frequency,  $c_1$  and  $c_2$  the shear wave speeds in the upper and the lower compartments, and  $\hat{\mathbf{y}}$  denotes the Cartesian unit vector in the corresponding direction. In the MRE experiments the angular frequency is determined by the external driving frequency  $f$  of the vibrator ( $\omega = 2\pi f$ ). The reflection and transmission coefficients  $R$  and  $T$  can now be directly calculated by imposing boundary conditions at the elastic interface. Assuming continuity of displacement and traction would model a welded interface. To model a nonwelded interface, it is necessary to consider slip. In terms of boundary conditions this means that the displacement must be allowed to be discontinuous at the interface. According to Schoenberg (1980), the difference in displacement between the two compartments is assumed to be proportional to the induced surface traction  $\tau_{yz}$ , while this traction component is assumed to be continuous. The boundary conditions at  $z = 0$  then read

$$u_{y2} - u_{y1} = \xi \tau_{yz1,2} \quad \text{and} \quad \tau_{yz2} - \tau_{yz1} = 0, \quad (2)$$

where  $\xi$  is the specific compliance of the interface, which is the inverse-specific stiffness  $\kappa = 1/\xi$  attributed to the interface, and

$$\tau_{yz1,2} = \rho_{1,2} c_{1,2}^2 \frac{\partial u_{y1,2}}{\partial z} \quad (3)$$

is the component of the stress tensor that gives the only nonzero component of the vector of traction. Here, the Arabic index refers to the elastic half-space, the Latin indices label the Cartesian components of displacement and traction, and  $\rho$  is the density of the material. The traction (3) in either compartment can be chosen to evaluate the right-hand side of the first equation in (2). Inserting (1) into (2) yields for  $R$  and  $T$

$$R = \frac{\rho_1 c_1 \cos \alpha_1 - \rho_2 c_2 \cos \alpha_2 - \Delta}{\rho_1 c_1 \cos \alpha_1 + \rho_2 c_2 \cos \alpha_2 - \Delta}, \quad T = \frac{2\rho_1 c_1 \cos \alpha_1}{\rho_1 c_1 \cos \alpha_1 + \rho_2 c_2 \cos \alpha_2 - \Delta}, \quad (4)$$

where

$$\Delta = i\xi\omega\rho_1\rho_2c_1c_2\cos\alpha_1\cos\alpha_2,$$

and  $|T + R| = 1$ . Setting  $\xi = 0$  reproduces the result for SH-wave scattering from a welded surface (Aki and Richards 2002). The absolute values of the scattering coefficients as a function of the angle of incidence are shown in figure 2. In this paper, only waves normally incident on the interface are studied as a function of frequency. At small angles of incidence the cos-terms are approximately one, and if the two compartments are identical, i.e.  $c_1 = c_2 = c$  and  $\rho_1 = \rho_2 = \rho$ , (4) is further reduced to

$$R = \frac{-i\xi\omega\rho c}{2 - i\xi\omega\rho c}, \quad T = \frac{2}{2 - i\xi\omega\rho c}. \quad (5)$$

Since the coefficients are complex, they can be expressed as the product of their absolute value and the corresponding phase factor. For the reflection coefficient  $R$  one finds

$$R = |R|e^{i\phi_r}, \quad \phi_r = -\frac{2}{\xi\omega\rho c}, \quad |R| = \frac{\xi\omega\rho c}{\sqrt{4 + \xi^2\omega^2\rho^2c^2}}, \quad (6)$$

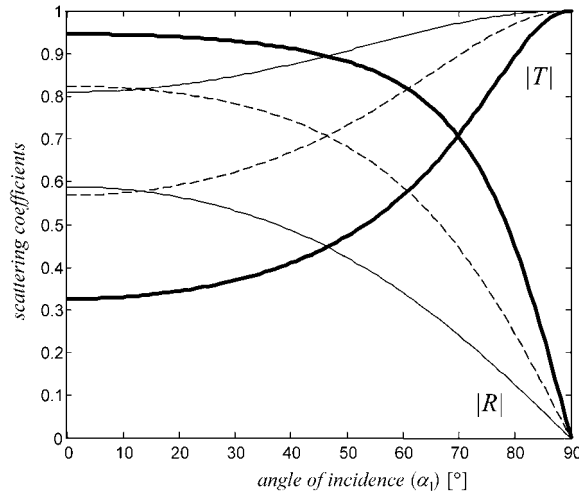


**Figure 2.** Angular dependence of the reflection coefficient  $|R|$  and the transmission coefficient  $|T|$  corresponding to (4) at three different vibration frequencies: 50 Hz (thin solid line), 100 Hz (dashed line), 200 Hz (fat solid line). The material was assumed to be identical on both sides of the interface with  $c_1 = c_2 = 3.3 \text{ m s}^{-1}$  and  $\rho_1 = \rho_2 = 1000 \text{ kg m}^{-3}$ . The specific stiffness of the contact was  $\kappa = 0.7 \text{ kPa mm}^{-1}$ .

and the transmission coefficient is

$$T = |T| e^{i\phi_t}, \quad \phi_t = \frac{1}{2} \xi \omega \rho c, \quad |T| = \frac{2}{\sqrt{4 + \xi^2 \omega^2 \rho^2 c^2}}. \quad (7)$$

If  $\epsilon = \xi \omega \rho c$  is introduced as a small dimensionless parameter one finds the asymptotic low nonweldedness or low-frequency behaviour ( $\epsilon \rightarrow 0$ )

$$|R| \approx \frac{1}{2} \epsilon - O(\epsilon^3), \quad |T| \approx 1 - O(\epsilon^2), \quad (8)$$

for the scattering coefficients. These results show that at very low frequencies, only a transmitted wave exists, having the same amplitude as the incident wave and no change in its phase. The behaviour is as if the contact had been welded. On the other hand, it is apparent that the amplitude of the transmitted wave is suppressed at high frequencies, thus providing a low-pass filter for SH-wave scattering. Moreover, the phase shift is always positive for the transmitted and negative for the reflected wave. The coefficients  $R$  and  $T$  as given by (5) can also be deduced from a three-layer model, which provides some more physical insight into the mechanism of SH-wave energy transport through an interface. The corresponding equations are given in the appendix.

### 3. Methods

MR experiments were performed using a standard head coil of a 1.5 T MR scanner (Sonata, Siemens, Erlangen, Germany). A modified EPI sequence (Hamhaber *et al* 2007) was used that incorporates motion sensitization gradients along the direction of slice selection ( $y$ -direction) and  $xz$  image plane according to figure 1. Twenty time steps were recorded that encompass a whole vibration cycle with toggled motion sensitization gradients at each second image. Shear waves were induced by a transducer plate on top of the phantom (figure 3) driven by an acousto-mechanical vibration generator outside of the magnet (Klatt *et al* 2006). A  $13.5 \times 13.5 \times$

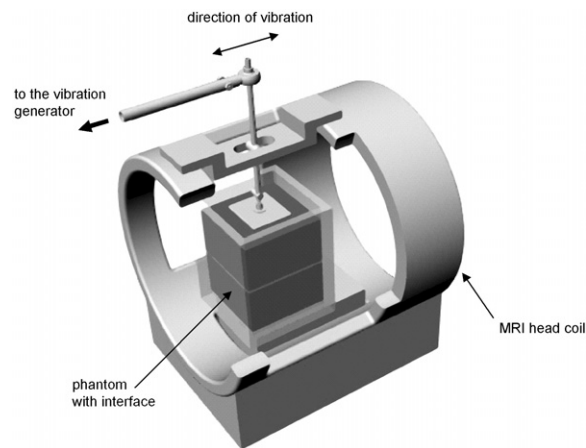


**Figure 3.** Experimental setup of MR elastography phantom experiments.

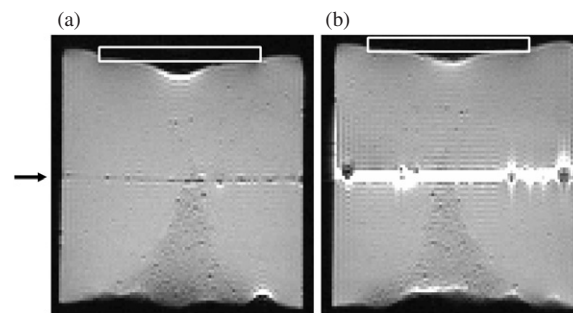


**Figure 4.** MRI magnitude images of a homogeneous phantom that includes an interface which behaves either welded (a) or nonwelded (b) in the vibration frequency range of this study. The arrow indicates the position of the welded interface. In (b) the nonwelded interface is well visible as an intense signal of the aqua gel layer (thickness  $d \approx 4$  mm), which is caused by a larger  $T_2$  relaxation time than in the surrounding phantom. The position of the transducer plate is demarcated at the upper boundary.

14 cm gel phantom (Wirogel, Bego Inc., Bremen, Germany, water = 1/3) was horizontally cut into two equal-sized compartments. In a first experiment, the two compartments were directly in contact welded by static friction. In a second experiment, an approximately 4 mm thick layer of aqua gel (SteriPharm, Berlin, Germany) was introduced to allow both compartments to slip against each other (figure 4). In the following both kinds of interfaces are referred to as being the ‘welded’ and ‘nonwelded’ contact, respectively. The shear wave excitation frequency was 100, 200, 300 and 400 Hz for the phantom with the welded interface and 50, 60, 75, 90, 100, 150, 200, 300 and 400 Hz for the nonwelded contact phantom. The shear wave speed of the layer was determined in a separate experiment by exciting a container of aqua gel using vibration frequencies of 75, 100 and 150 Hz.

A spatio-temporal directional filtering of the three-dimensional wave data  $u(x, z, t)$  was used to separate the incident and transmitted waves (waves with no direction components from bottom to top) from those reflected by the contact interface and the bottom of the container (waves with no direction components from top to bottom). First the data was Fourier-

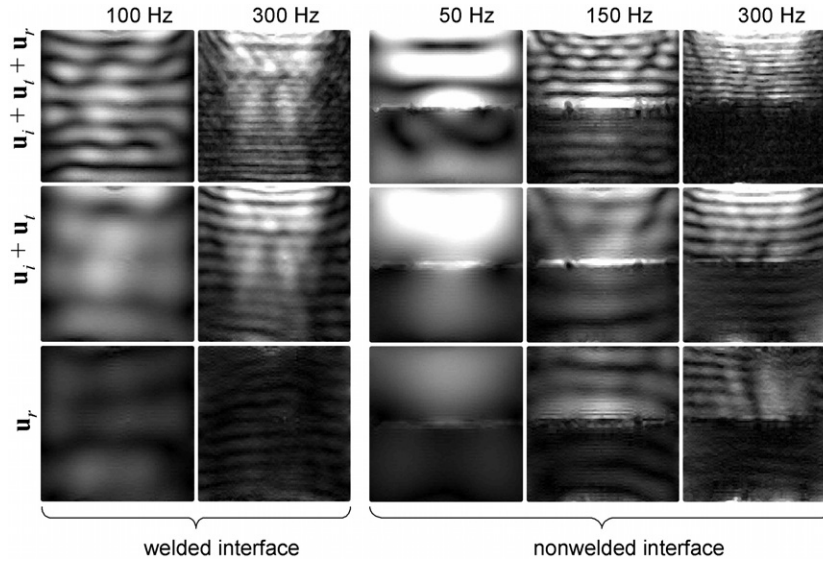


**Figure 5.** Magnitude images of SH-waves ( $|\hat{u}(x, z, \omega)|$ ) due to different vibration frequencies (given above the images) which travel through a welded and a nonwelded contact surface. The first row shows  $|\hat{u}(x, z, \omega)|$  of the originally acquired data. The second and third rows show spatio-temporally filtered data, for extracting the downwards or upwards running wave, respectively.

transformed from the position time-domain ( $\mathbf{r}, t$ ) to the wave number frequency-domain ( $\mathbf{k}, \omega$ ). Similar to Manduca *et al* (2003), the Fourier half-spaces were filtered using two symmetrically mirrored directional filters with  $\cos^2$  dependence with respect to the direction of  $\mathbf{k}$ . The filtered images were inversely Fourier-transformed with respect to  $\mathbf{k}$ .

The obtained wave images  $\hat{u}(x, z, \omega)$  were then used to determine  $|T|$  and  $|R|$  by means of the magnitudes of the amplitudes ( $|\hat{u}(x, z, \omega)|$ ) of transmitted and reflected waves normalized to the incident wave. Thus,  $|\hat{u}(x, z, \omega)|$  was averaged over a small spatial region of  $\Delta x = 1.4$  cm and  $\Delta z = 4.2$  cm located at the centre of the phantom directly above or beneath the interface for determining  $|R|$  or  $|T|$ . The scattering coefficients  $|R|$  and  $|T|$  were fitted using equations (6) and (7) with varying  $\kappa$  by minimizing the squared deviation between calculated curve and experiments. For error estimates, upper and lower boundaries of  $\kappa$  are given which confine all experimental data points aside from single mavericks. Further simulation parameters were:  $c = 3.3$  m s $^{-1}$ ,  $\rho = 1000$  kg m $^{-3}$ .

#### 4. Results

Figure 5 shows sample images of the wave magnitudes in both phantoms with welded and nonwelded interfaces. Wave speeds of the phantom gel matrix and layer material were determined with  $3.3 \pm 0.2$  m s $^{-1}$  and  $0.9 \pm 0.2$  m s $^{-1}$ , respectively. The first row in figure 5 shows the magnitudes of the superposed incident, transmitted and reflected waves. It can be seen that the welded interface barely influences the wave amplitudes, whereas the nonwelded contact acts as a low-pass filter rejecting higher vibration frequencies. This behaviour is even better illustrated by the second and third rows of figure 5. There, the downward- and upward-running waves are separated, yielding amplitudes for the incident and the transmitted waves in the second row and the reflected waves in the bottom row. The amplitudes of the

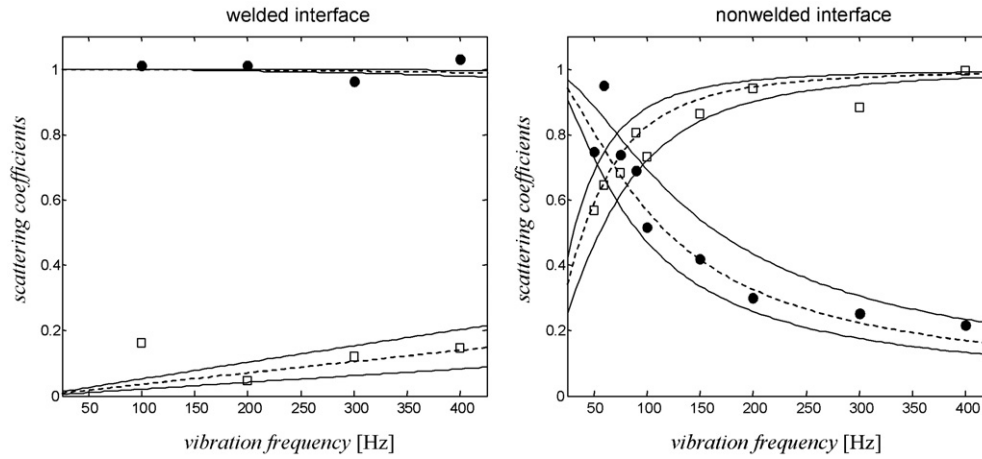


**Figure 6.** Scattering coefficients  $|R|$  ( $\square$ ) and  $|T|$  ( $\bullet$ ) according to equations (6) and (7) for the welded and the nonwelded interfaces measured by MR elastography experiments. The dashed lines indicate the best match in a least-squares sense of the experimental data to the linear slip model, while the solid lines provide error margins.

transmitted waves do not significantly change while travelling through the welded interface. In contrast, a drop of wave amplitude beneath the nonwelded interface is visible at 300 Hz. The upward-running wave magnitudes clearly show reflections at the bottom of the vessel. Such reflections are increasingly suppressed at higher vibration frequencies as a result of the nonwelded contact interface and viscosity of the phantom. Figure 6 shows the reflection and transmission coefficients as functions of the frequency. The data were fitted using  $\kappa = 30 \text{ kPa mm}^{-1}$  for the welded contact and  $0.7 \text{ kPa mm}^{-1}$  for the nonwelded contact. The upper and lower error margins are given with  $50$  and  $20 \text{ kPa mm}^{-1}$  for the welded contact and  $1.0$  and  $0.5 \text{ kPa mm}^{-1}$  for the nonwelded interface. These margins do not confine the experimental transmission coefficient of the welded contact. Figure 6 shows that in the range of small  $\epsilon$  given by the welded interface the linear approximation of equations (8) is well applicable.  $|T|$  shows no significant variation with vibration frequency which increases the tolerance of the fit of  $\kappa$ .

Figure 7 shows the scattering coefficients using the three-layer model as given in (A.2) in the appendix. Viscosity was included according to (A.4). The transmission coefficient was fitted by changing  $c_0$  and  $\eta$  in equation (A.2) in a least-squares minimization routine. Best fit values were  $c_0 = 1.7 \pm 0.4 \text{ m s}^{-1}$  and  $\eta = 3.6 \pm 0.4 \text{ Pa s}$ . The shown reflection coefficient corresponds to these values. Using the fitted  $c_0$  as  $\bar{c}$  (representing the limit  $f = 0$ ) and an approximate layer thickness of the intermediate layer of  $4 \text{ mm}$  allows us to recalculate  $\kappa$  from (A.3) with  $\kappa(f = 0) = 0.6 \pm 0.2 \text{ kPa mm}^{-1}$ . While this value agrees to the linear slip model,  $c_0$  is larger than the experimentally observed shear wave speed of the layer material ( $0.9 \pm 0.2 \text{ m s}^{-1}$ ). This difference increases with frequency as a result of viscosity, which is opposed to the experimental findings where no wave speed dispersion was observed.

## 5. Discussion

We demonstrated for the first time experiments to measure the weldedness of soft materials by shear wave scattering. The results agree with theoretical predictions of SH-wave scattering

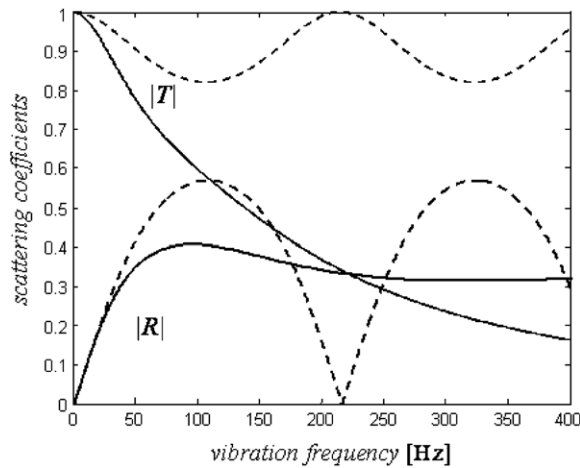


**Figure 7.** Scattering coefficients  $|R|$  and  $|T|$  according to a three-layer model (equations (A.2)) without viscosity (dashed lines) and including viscosity (solid lines).

from a linear slip interface in the dynamic range of *in vivo* MR elastography. In this model, the weldedness of two layers is deduced from the discontinuity of wave amplitudes at an interface and the traction across this interface. These quantities are combined in  $\kappa$  as a phenomenological means for characterizing interfaces and elastic contacts in elastography. However,  $\kappa$  provides only limited insight into the elastic properties of the underlying materials. Therefore, Schoenberg (1980) introduced the three-layer model given in the appendix. There,  $\kappa$  is related to the stiffnesses of an intermediate layer, the surrounding medium and the thickness of the layer. If the thickness is small compared to the length of shear waves, equation (A.3) is valid. However this limit is exceeded by the frequency range examined in this study as demonstrated in figure 7. Resonances of the scattering coefficients characterized by maximum transmission and no reflection of wave energy at integer multiples of  $f = \bar{c}/2d$  were not seen in our experiments. Figure 7 further illustrates that such resonances can be suppressed if viscosity is taken into account as given by equation (A.4). A transmission coefficient similar to that of the linear slip model is obtained at a viscosity of 3.6 Pa s. However, the loss of wave energy shown by the low reflection coefficient in figure 7 indicates that  $\eta$  is presumably overestimated and there are further transport mechanisms of wave energy through the interface. Also the discrepancy between experimental and fitted  $c_0$  indicates the limited applicability of (A.3) for explaining the physical meaning of  $\xi$  or  $\kappa$ . In our analysis, wave amplitudes were related to SH-wave scattering, assuming an alignment of the plane wave driver parallel to the interface and the corresponding adjustment of the scanner frame. Although the experimental setup was optimized to solely capture SH-waves, a small contribution of P- and SV-waves to the wave images as shown in figure 5 cannot entirely be excluded. In more realistic situations, the existence of multiple interfaces in oblique positions to each other would prevent a distinction between SH- and SV-waves as made in this study. For instance, in human brain MR elastography, sulci, blood vessels and interfaces between grey and white matter cause multiple scattering of shear waves with unclear directionality and polarization of the incident and the reflected waves. The quantification of *in vivo* scattering experiments is thus more complex and cannot be solved by the equations used in this study. On the other hand, the quality of amplitude variations can be utilized to identify the location of interfaces in complex

media as reported by Sack *et al* (2006). This observation agrees well with the wave images shown in figure 5 where the nonwelded interface is clearly distinguishable by means of steep amplitude changes.

In summary, we introduced a method for measuring SH-wave scattering in MR elastography. The method utilizes directional filtering of shear waves to separate incident and transmitted waves from back-running reflections in the vicinity of interfaces. Such separate wave components enable the measurement of scattering coefficients which in turn reveal mechanical tissue parameters such as acoustic impedance or the connectivity of interfaces.

## Appendix

For deducing the scattering coefficients by a three-layer model based on Schoenberg (1980) an intermediate layer with two welded contacts is assumed. Again, only normally incident waves are considered and the density of material is assumed to be the same for all layers. The involved plane waves read

$$\begin{aligned} u_{y1} &= \exp(i\omega z/c) + R \exp(-i\omega z/c), & z > d, \\ u_{y2} &= A \cos(\omega z/\bar{c}) + B \sin(\omega z/\bar{c}), & d > z > 0, \\ u_{y3} &= T \exp(i\omega(z-d)/c), & z < 0, \end{aligned} \quad (\text{A.1})$$

where  $\bar{c}$  is the shear wave velocity of the intermediate layer,  $d$  is its thickness and  $c$  is the shear wave speed of the surrounding layers. The coefficients  $A$  and  $B$  correspond to the wave amplitudes inside the intermediate layer. Applying boundary conditions for a welded contact (see (2) with  $\xi = 0$ ) yields the reflection and transmission coefficients

$$\begin{aligned} R &= \frac{(\bar{c}^2 - c^2) \sin(\omega d/\bar{c})}{2i\bar{c}c \cos(\omega d/\bar{c}) + (\bar{c}^2 + c^2) \sin(\omega d/\bar{c})} \\ T &= \frac{2i\bar{c}c}{2i\bar{c}c \cos(\omega d/\bar{c}) + (\bar{c}^2 + c^2) \sin(\omega d/\bar{c})}. \end{aligned} \quad (\text{A.2})$$

At low frequencies, when  $d$  is small compared to the shear wave length, the sin-terms can be replaced by their argument and the cos-terms are equal to 1. Equations (5) are then reproduced with

$$\xi = \frac{d}{\rho\bar{c}^2} \left( 1 + \frac{\bar{c}^2}{c^2} \right). \quad (\text{A.3})$$

For a viscous intermediate layer the velocity  $\bar{c}$  can be replaced according to Voigt's model of a viscoelastic body (Fung 1993) by

$$\bar{c} = \left( c_0^2 - \frac{i\omega\eta}{\rho} \right)^{1/2}, \quad (\text{A.4})$$

where  $c_0$  is the shear wave velocity obtained in the limit  $\omega \rightarrow 0$  and  $\eta$  is the viscosity.

## References

- Aki K and Richards P G 2002 *Quantitative Seismology* (Sausalito, CA: University Science Books)
- Chaisri S and Krebes E S 2000 Exact and approximate formulas for P-SV reflection and transmission coefficients for a nonwelded contact interface *J. Geophys. Res.* **105** 28045–54
- Fung Y C 1993 *Biomechanics* (New York: Springer)
- Hamhaber U, Sack I, Papazoglou S, Rump J, Klatt D and Braun J 2007 Three-dimensional analysis of shear wave propagation observed *in vivo* magnetic resonance elastography of the brain *Acta Biomater.* **3** 127–37

- Klatt D, Asbach P, Rump J, Papazoglou S, Somasundaram R, Modrow J, Braun J and Sack I 2006 *In vivo* determination of hepatic stiffness using steady-state free precession magnetic resonance elastography *Invest. Radiol.* **41** 841–8
- Lerner R M, Huang S R and Parker K J 1990 Sonoelasticity images derived from ultrasound signals in mechanically vibrated tissues *Ultrasound Med. Biol.* **16** 231–39
- Manduca A, Lake D S, Kruse S A and Ehman R L 2003 Spatio-temporal directional filtering for improved inversion of MR elastography images *Med. Image Anal.* **7** 465–73
- Muthupillai R, Lomas D J, Rossman P J, Greenleaf J F, Manduca A and Ehman R L 1995 Magnetic resonance elastography by direct visualization of propagating acoustic strain waves *Science* **269** 1854–57
- Park E and Maniatty A M 2006 Shear modulus reconstruction in dynamic elastography: time harmonic case *Phys. Med. Biol.* **51** 3697–721
- Pyrak-Nolte L J, Myer L R and Cook N G W 1990 Transmission of seismic waves across single natural fractures *J. Geophys. Res.* **95** 8617–38
- Sack I, Papazoglou S, Hamhaber U, Klatt D, Rump J and Braun J 2005 Shear wave scattering in MR elastography: detection of elasticity interfaces *Proc. Int. Soc. Mag. Reson. Med.* **13** 615
- Sack I, Rump J, Papazoglou S, Klatt D, Hamhaber U, Gedat E and Braun J 2006 Shear-wave scatter contrast enhancement in steady-state MR elastography *Proc. Int. Soc. Mag. Reson. Med.* **14** 912
- Sandrin L, Catheline S and Fink M 1999 Transient elastography in biological tissues *J. Acoust. Soc. Am.* **105** 1014–15
- Schoenberg M 1980 Elastic wave behavior across linear slip interfaces *J. Acoust. Soc. Am.* **68** 1516–21
- Slawinski R A and Krebes E S 2002 Finite-difference modeling of SH-wave propagation in nonwelded contact media *Geophysics* **67** 1656–63
- Tibikram K 2004 *Ultrasonic Nondestructive Evaluation* (Boca Raton, FL: CRC Press)
- Verweij M D and Chapman C H 1997 Transmission and reflection of transient elastodynamic waves at a linear slip interface *J. Acoust. Soc. Am.* **101** 2473–84